

# Quantum Monte Carlo study of strange correlator in interacting topological insulators

Han-Qing Wu,<sup>1</sup> Yuan-Yao He,<sup>1</sup> Yi-Zhuang You,<sup>2</sup> Cenke Xu,<sup>2</sup> Zi Yang Meng,<sup>3,\*</sup> and Zhong-Yi Lu<sup>1</sup>

<sup>1</sup>*Department of Physics, Renmin University of China, Beijing 100872, China*

<sup>2</sup>*Department of Physics, University of California, Santa Barbara, California 93106, USA*

<sup>3</sup>*Beijing National Laboratory for Condensed Matter Physics,*

*and Institute of Physics, Chinese Academy of Sciences, Beijing 100190, China*

(Dated: December 3, 2024)

Distinguishing nontrivial symmetry protected topological (SPT) phase from trivial insulator in the presence of electron-electron interaction is an urgent question to the study of topological insulators, due to the fact that most of the topological indices defined for free electron systems are very likely unsuitable for interacting cases. In this work, we demonstrate that the strange correlator is a sensitive diagnosis to detect SPT states in interacting systems. Employing large-scale quantum Monte Carlo (QMC) simulations, we investigate the interaction driven quantum phase transition in the Kane-Mele-Hubbard model. The transition from quantum spin Hall insulator at weak interaction to antiferromagnetic Mott insulator at strong interaction can be readily detected by the momentum space behavior of the strange correlator in single-particle, spin, and pairing sectors. The interaction effects on the symmetry-protected edge states in various sectors, *i.e.*, the helical Luttinger liquid behavior, are well captured in the QMC measurements of strange correlators. Moreover, we demonstrate that the strange correlator is technically easier to implement in QMC and robuster in performance than other proposed numerical diagnoses for interacting SPT states, as only static correlations are needed. The attempt in this work paves the way for using the strange correlator to study interaction driven topological phase transitions in fermionic as well as bosonic systems.

PACS numbers: 71.10.-w, 71.10.Fd, 71.27.+a

## I. INTRODUCTION

Topological insulators (TI), or more generally symmetry protected topological (SPT) states<sup>1,2</sup>, are usually defined as systems with bulk spectra similar to those of trivial insulator, but with nontrivial, *i.e.* gapless or degenerate, boundary spectrum when and only when the systems (including the boundaries) preserve certain symmetries. By now the noninteracting TIs have been fully classified and understood, for example, as shown in Refs. 3–5. Besides the boundary states which are experimentally most relevant, the noninteracting TIs can also be characterized by a topological index defined for the bulk band structure, namely, even if a TI has the similar bulk spectrum as a trivial insulator, it does have very different ground state wave function which is characterized by the topological indices, for example, the TKNN number for the integer quantum Hall state<sup>6</sup> and the  $Z_2$  index for quantum spin Hall insulator<sup>7,8</sup>. But so far most of the techniques and topological indices introduced for noninteracting topological insulators are very likely unsuitable for interacting cases, since in many cases interaction can change (or reduce) the classification of topological insulators<sup>9–19</sup>. Thus a more general technique to identify interacting TIs (or SPT states) based on their bulk wave functions is urgently demanded for studying of topological insulators in the presence of electron-electron interactions.

In principle, given a bulk wave function, we can always compute its entanglement spectrum and use it as a diagnosis for interacting TI<sup>20</sup>. However, this technique is numerically challenging. For strongly correlated electron

systems, in one dimension (1D) we are able to obtain the bulk wave function and entanglement spectrum from exact diagonalization (ED) and density matrix renormalization group (DMRG) calculations, but in two (2D) and higher dimensions, it is very difficult to obtain the bulk wave functions for interacting systems simply because the dimension of Hilbert space increases exponentially with the number of electrons. In 2D, there are recent progresses by employing quantum Monte Carlo simulations to access the entanglement spectrum<sup>21–23</sup>, but the approach is arduous as one needs to first bifurcate the already small finite-size system (the simulation efforts of QMC scale polynomially with system size to high power), and then perform analytical continuation to obtain real frequency entanglement spectrum from the reduced density matrix in imaginary time<sup>22,23</sup>. The analytical continuation<sup>24,25</sup>, as useful as it is, is a numerically ill-posed question and warned for bringing ambiguities that mask the fine features in the real frequency data. These difficulties shadow the progress in evaluating the bulk wave functions and entanglement information for diagnosing interacting TIs.

In light of the difficult situation for interacting TIs, recently, a new diagnosis dubbed “strange correlator” was proposed in Ref. 26, which is the matrix element of the correlation function between two topologically distinct many-body bulk wave functions in the same Hilbert space. Based on the low energy effective Lorentz invariance of the SPT states, the strange correlator, though it is a purely static quantity, effectively captures the space-time correlation function at the spatial interface between the two topologically distinct phases. Hence, as long as there exist symmetry-protected edge states at the spa-

tial interface, i.e., the two wavefunctions are topologically distinct, the strange correlator will diagnose the edge modes, at least for the non-interacting case. As will become clear in this paper, for the QMC simulations for interacting TIs, the strange correlator can diagnose the correlated edge modes as well. Moreover, as the strange correlator is based on the bulk wave function, there is no need to explicitly create a real spatial boundary to detect the gapless edge modes, which, in interacting systems, usually gives rise to strong finite size effects. Also, comparing with the measurements of entanglement spectrum mentioned above, there is no need to bifurcate the system for evaluating the strange correlators. There is also no need to perform imaginary-time correlation as the strange correlators are static quantities which avoids the analytical continuation step. These advantages make strange correlator physically transparent and technically much easier to implement in QMC. Yet another advantage of strange correlator is that it is generally applicable to both fermionic and bosonic SPT states, either free or interacting. It is also applicable to “crystalline” TI<sup>27</sup>, because it respects all the lattice symmetries (no need for boundaries).

In Ref. 26, the strange correlator has only been applied to free fermion topological insulators and some bosonic SPT states. Later on, in Ref. 28 and 29, it was demonstrated that the strange correlator can capture the nature of the Haldane phase of 1D spin-1 system. It was further shown in Ref. 30 that the strange correlators of 2D bosonic SPT states can be expressed as correlation functions of 2D conformal field theory. However, the most important test, namely, the application of strange correlator upon interacting fermion topological insulators to diagnose the interaction driven topological phase transition, has never been performed. Here, by means of large-scale quantum Monte Carlo simulations, we apply the strange correlator to a very realistic and nonintegrable model for interacting topological insulator, namely the Kane-Mele-Hubbard model. We present in details on how to evaluate the strange correlators in determinantal QMC<sup>31</sup> simulations for interacting fermionic systems, and use it to probe the topological nature of the interaction-driven quantum phase transition in the KMH model. Furthermore, the interaction effects on the helical edge states – the Luttinger liquid behavior, have been also clearly captured by the strange correlator measurements in QMC simulations.

The rest of the paper is organized as follows. In Sec. II the KMH model (II A) and strange correlators in various sectors (II B) are introduced, with detailed account on their implementation in QMC simulations. In Sec. III, the strange correlator in single-particle sector (III A) is first demonstrated, followed by those in two-particle spin and pairing sectors (III B). In the single-particle sector, the topological nature of the quantum spin Hall insulator to antiferromagnetic Mott insulator transition can be clearly seen. In the two-particle channel, the Luttinger liquid behavior of the edge modes, are well captured

by their corresponding QMC strange correlator measurements. Sec. IV summarizes the physical and numerical advantages of strange correlator in diagnosing interacting TIs and proposes future directions.

## II. MODEL AND NUMERICAL METHOD

### A. generalized Kane-Mele-Hubbard model

The generalized Kane-Mele-Hubbard (KMH) model is given by,

$$H_{\text{KMH}} = - \sum_{\langle i,j \rangle, \sigma} t_{ij} c_{i\sigma}^\dagger c_{j\sigma} + i\lambda \sum_{\langle\langle i,j \rangle\rangle, \alpha\beta} v_{ij} c_{i\alpha}^\dagger \sigma_{\alpha\beta}^z c_{j\beta} + \frac{U}{2} \sum_i (n_i - 1)^2. \quad (1)$$

Here the first term describes the nearest-neighbor hopping on a honeycomb lattice. As shown in Fig. 1 (a), we set the nearest-neighbor hopping within one unit cell with amplitude  $t_d$ , while others with amplitude  $t$ .  $t_d$  and  $t$  can be different, depending on the context. The second term represents spin-orbit coupling<sup>7,8</sup>, which connects the next-nearest-neighbor sites with a complex (time-reversal symmetric) hopping with amplitude  $\lambda$ , and the factor  $v_{ij} = -v_{ji} = \pm 1$  depends on the orientation of the two nearest neighbor bonds that the electron traverses in going from site  $j$  to  $i$ . The  $\sigma_{\alpha\beta}^z$  in the spin-orbit coupling term furthermore distinguishes the  $\uparrow$  and  $\downarrow$  spin states with the opposite next-nearest-neighbor hopping amplitudes.

Physically, the non-interacting ( $U = 0$ ) Kane-Mele (KM) model<sup>7,8</sup> is a spinful model consisting of two copies of the the Haldane model<sup>32</sup> with opposite spins. Although the spinless Haldane model breaks the time-reversal symmetry  $Z_2^T$ , the spinful KM model is time-reversal invariant and its ground state is a quantum spin Hall (QSH) insulator with counter propagating edge modes. Regarding the symmetries of the KMH model, the model Hamiltonian in Eq. 1 has the charge  $U(1)_{\text{charge}}$  symmetry:  $c_{i\sigma} \rightarrow e^{i\theta} c_{i\sigma}$ . The spin-rotational symmetry  $SU(2)$  is broken down by the spin-orbit coupling (SOC) term  $\lambda$  to  $U(1)_{\text{spin}}$ , which only keeps the spin rotation in the  $xy$  plane:  $c_{i\sigma} \rightarrow e^{i\sigma\theta} c_{i\sigma}$ . So the symmetry group of the KMH model is  $U(1)_{\text{charge}} \times U(1)_{\text{spin}} \rtimes Z_2^T$ , which results in a  $\mathbb{Z}$  classification. This implies that the QSH state must be separated from the trivial vacuum state with gapless edge modes.

In the presence of interaction, the KMH model can be studied by determinantal QMC simulations<sup>31,33–40</sup>. At the non-interacting limit,  $U = 0$ , for any finite  $\lambda$ , the system is in the QSH state at zero temperature. Switching on finite but weak interaction ( $U/t > 0$ ), the system is adiabatically connected to the noninteracting QSH. At strong interaction,  $U/t$  will drive the QSH state into an antiferromagnetic ordered Mott insulator (AFMI) state<sup>41</sup>, through a continuous quantum phase transition

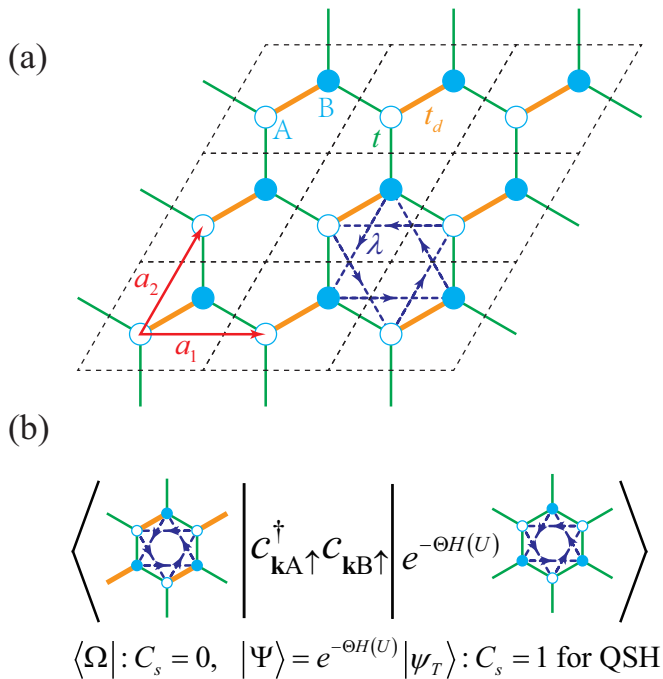


FIG. 1. (color online) (a) Illustration of honeycomb lattice and Kane-Mele model. The unit cell of honeycomb lattice is presented as the dashed black parallelogram, it consists of two sublattices A, B, denoted by the open and filled cyan circles. The underlying lattice is spanned by the primitive vectors  $a_1 = (\sqrt{3}, 0)$ ,  $a_2 = (1/2, \sqrt{3}/2)$ . The green and orange lines represent nearest-neighbor hopping  $t$  and  $t_d$  connecting the A and B sublattices. The spin-orbital coupling term (complex valued next-nearest-neighbor spin-dependent hopping  $i\lambda$ ) connects lattices sites within the same sublattice, and is denoted as the blue dashed arrows. (b) Schematic plot of  $|\Omega\rangle$  and  $|\Psi\rangle$  in single-particle strange correlator calculation, where  $|\Omega\rangle$  is a trivial band insulator with spin Chern number  $C_s = 0$  and the detected target state  $|\Psi\rangle$  is the many-body ground wave function of KMH Hamiltonian in Eq. 1 evaluated in the QMC simulation. It is prepared by applying projection operator  $e^{-\Theta \hat{H}}$  onto a non-interacting trival wave function  $|\Psi_T\rangle$  (eigenstate of KM model with  $U = 0$ ). The topological nature of  $|\Psi\rangle$  depends on the interaction strength  $U/t$ , when  $U \leq U_c$  the system is in the QSH insulator phase with spin Chern number  $C_s = 1$ , but when  $U > U_c$ , the system is the AFMI phase, which spontaneously breaks the key symmetry that protects the topological insulator.

at critical point  $U_c$  (e.g., at  $\lambda = 0.1t$ ,  $U_c \sim 5t$ ). At the transition, the single-particle gap remains open, but the corresponding spin gap closes<sup>35,37,40</sup>. The transition from the QSH to the  $xy$  AFMI has been shown to be consistent with the 3D XY universality class<sup>35,36,42</sup>. As both  $U(1)_{\text{spin}}$  and  $Z_2^T$  symmetries are spontaneously broken in the AFMI phase, only  $U(1)_{\text{charge}}$  remains. Meanwhile there is another time-reversal-like symmetry  $Z_2^{T'}$ :  $c_{i\alpha} \rightarrow \mathcal{K} \sigma_{\alpha\beta}^x c_{i\beta}$ , so the total remaining symmetry is  $U(1)_{\text{charge}} \times Z_2^{T'}$  with  $\mathcal{T}^2 = 1$  and the fermion SPT classification becomes trivial, as such a time-reversal-

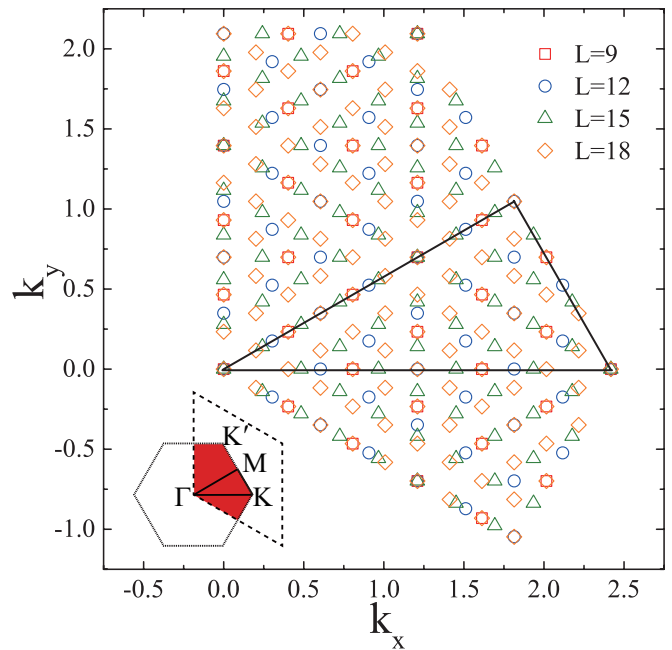


FIG. 2. (color online) Illustration of the  $\mathbf{k}$ -mesh in the Brillouin zone (BZ) of finite-size systems studied in QMC simulations with linear system size  $L = 9, 12, 15, 18$ . The black line is the high-symmetry paths  $\Gamma \rightarrow M \rightarrow K \rightarrow \Gamma$ . As  $L$  increases, the  $\mathbf{k}$ -mesh becomes denser. The inset is the hexagon BZ of honeycomb lattice and the shaded region represents the segment of the BZ shown in the main panel.

like symmetry with  $\mathcal{T}^2 = 1$  does not lead to Kramers doublet. This means if we neglect the Goldstone mode in the bosonic sector, the AFMI state must belong to the trivial SPT class which can be smoothly connected to a trivial band insulator (such as a spin density wave (SDW) insulator) in the fermionic sector. So there is no symmetry-protected gapless fermionic edge mode between this AFMI and a trivial insulator.

## B. Strange correlator in QMC

To effectively diagnose the SPT states, the concept of strange correlator was proposed in Ref. 26. It is a correlation function defined between two many-body wave functions in the same Hilbert space,

$$C(r, r') = \frac{\langle \Omega | \phi(r) \phi(r') | \Psi \rangle}{\langle \Omega | \Psi \rangle}, \quad (2)$$

where  $|\Omega\rangle$  is a trivial band insulator, and  $|\Psi\rangle$  is the wave function whose topological nature we would like to diagnose. The physical meaning of  $C(r, r')$  becomes manifest after a space-time rotation<sup>26</sup>:  $|\Psi\rangle$  can be obtained by evolving a generic initial state from imaginary time  $\tau = -\infty$  to  $\tau = 0$  with the parent Hamiltonian of  $|\Psi\rangle$ , and  $|\Omega\rangle$  can be obtained by evolving a generic final state backward from imaginary time  $\tau = +\infty$  to  $\tau = 0$ , thus

$C(r, r')$  can be viewed as a correlation function at the temporal domain wall. Because most of the topological insulators have an effective Lorentz invariant description<sup>43</sup>, after a space-time rotation  $C(r, r')$  becomes the space-time correlation at the spatial interface between  $|\Psi\rangle$  and  $|\Omega\rangle$ , which may have gapless modes depending on the nature of the two states.

The proposition given in Ref. 26 is that if  $|\Psi\rangle$  is a nontrivial topological insulator (or more generally a SPT state) in one or two spatial dimension, i.e., there exist one or more gapless edge modes at the spatial boundary of  $|\Psi\rangle$ , then for local operator  $\phi(r)$  that transforms nontrivially under symmetry,  $C(r, r')$  will either develop long-range order (saturate to a *constant*) or decay as a power law in the limit  $|r - r'| \rightarrow +\infty$ , which mimics the edge states of  $|\Psi\rangle$ . In the momentum space, this corresponds to a singularity at certain symmetric momentum point  $\mathbf{k}_s$ :  $C_{\mathbf{k}} \sim 1/|\mathbf{k} - \mathbf{k}_s|^\alpha$ , if  $|\Psi\rangle$  is in a nontrivial topological insulator phase. Based on the space-time rotation argument given above, the 2D strange-correlator  $C(r, r')$  should behave very similarly to the (1+1)D correlation functions at the boundary. For example, if  $|\Psi\rangle$  is a generic *noninteracting* 2D TI, and  $\phi(r)$  is simply the electron operator, i.e.  $C(r, r') = \langle \Omega | c^\dagger(r) c(r') | \Psi \rangle / \langle \Omega | \Psi \rangle$ , then  $\alpha = 1$ . The strange correlator has been successfully applied to detect topological phase transitions in 1D and 2D spin systems<sup>26,28,29</sup>, as well as in non-interacting fermionic system<sup>26</sup>.

In our QMC simulations, to detect the correlated QSH phase and the interaction driven phase transition in the KMH model, we prepare  $|\Omega\rangle$  as the wave function of Eq. 1 with  $U = 0$ , but keep  $t_d$  different from  $t$ . At the non-interacting level, with finite  $\lambda$ ,  $t_d/t$  will drive a topological phase transition between QSH and trivial band insulator at  $t_d = 2t$ <sup>37,39,40</sup>, therefore, throughout this paper we choose  $|\Omega\rangle$  with  $\lambda = 0.2t$  and  $t_d = 100t$ , which guarantees it is a topologically trivial band insulator. On the other hand,  $|\Psi\rangle$  is prepared as the ground state wave function of interacting Hamiltonian in Eq. 1 with  $t_d = t$ . In the quantum Monte Carlo simulation, it is prepared as  $|\Psi\rangle = e^{-\Theta \hat{H}} |\Psi_T\rangle$ , where  $|\Psi_T\rangle$  is the wave function of noninteracting Hamiltonian in Eq. 1 with  $U = 0$ ,  $\lambda = 0.2t$  and  $t_d = t$ , the projection operator  $e^{-\Theta \hat{H}}$  is applied onto  $|\Psi_T\rangle$  in quantum Monte Carlo sampling such that when the projection parameter  $\Theta$  is sufficiently large, the QMC ensemble average guarantees  $|\Psi\rangle$  is the ground state of the interacting Hamiltonian  $\hat{H}$ . In most of the simulations, we set  $\Theta = 50t$ .

In this paper, we define the strange correlator in the momentum space. The strange correlator in single-particle channel for spin flavor  $\sigma$  is then defined as

$$C_{\mathbf{k}AB}^\sigma = \frac{\langle \Omega | c_{\mathbf{k}A\sigma}^\dagger c_{\mathbf{k}B\sigma} | \Psi \rangle}{\langle \Omega | \Psi \rangle}, \quad (3)$$

where  $c_{\mathbf{k}A\sigma}^\dagger = \frac{1}{L} \sum_i e^{i\mathbf{k}\cdot\mathbf{R}_{i,A}} c_{i,A,\sigma}^\dagger$  with  $\mathbf{k}$  inside the BZ shown in Fig. 2, and  $A, B$  are the two sublattices of the honeycomb lattice in Fig. 1 (a). The schematic plot of

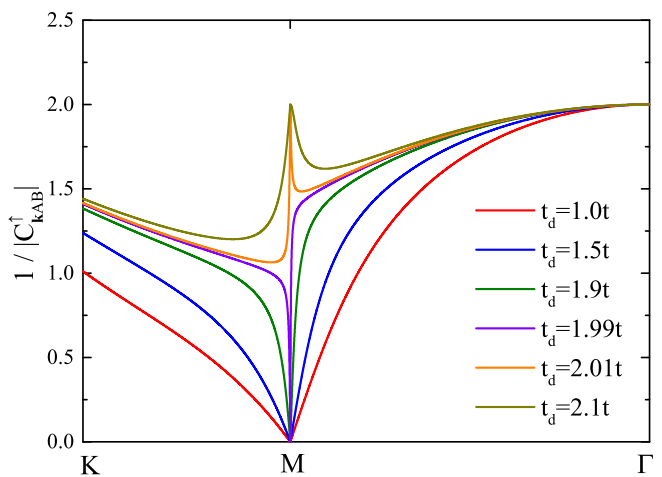


FIG. 3. (color online)  $1/|C_{\mathbf{k}AB}^\dagger|$  as a function of  $t_d$  in  $|\Psi\rangle$ . The linear divergence of  $|C_{\mathbf{k}AB}^\dagger|$  around M point holds robust until  $t_d > 2t$ . We can use the divergent to nondivergent behavior of  $|C_{\mathbf{k}AB}^\dagger|$  to determine the critical point precisely in this noninteracting case.

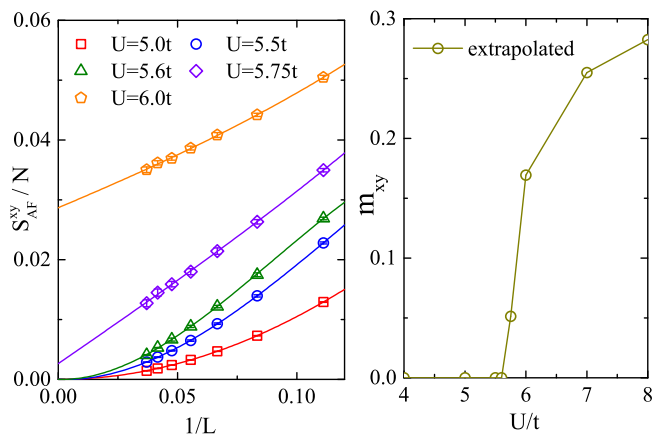


FIG. 4. (color online) (a). Finite size scaling of  $xy$  antiferromagnetic structure factor for various values of  $U/t$ , with linear system size  $L$  goes to 27. The extrapolated values of magnetic moment  $m_{xy}$  is plotted in (b).

Fig. 1 (b) depicts the idea of the strange correlator in KMH model, on the left hand side, the wave function  $|\Omega\rangle$  is a trivial band insulator (with spin Chern number  $C_s = 0$ ); on the right hand side, the projection operator  $e^{-\Theta \hat{H}}$  guarantees  $|\Psi\rangle = e^{-\Theta \hat{H}} |\Psi_T\rangle$  is the many-body ground state wave function of KMH Hamiltonian at certain  $U/t$ , although the trial wave function  $|\Psi_T\rangle$  is non-interacting (with spin Chern number  $C_s = 1$ ). In this way, as we gradually increase the interaction strength  $U/t$  in the KMH Hamiltonian, the nature of  $|\Psi\rangle$  will change from QSH at weak interaction ( $U \leq U_c$ ) to AFMI at strong interaction ( $U > U_c$ ).

We also measure the strange correlator in the spin and

Cooper-pair channels respectively as follows.

$$S_{\mathbf{k}AA}^{\pm} = \frac{\langle \Omega | S_{\mathbf{k}A}^{+} S_{\mathbf{k}A}^{-} | \Psi \rangle}{\langle \Omega | \Psi \rangle}, \quad (4)$$

$$D_{\mathbf{k}AA} = \frac{\langle \Omega | \Delta_{\mathbf{k}A}^{\dagger} \Delta_{\mathbf{k}A} | \Psi \rangle}{\langle \Omega | \Psi \rangle}, \quad (5)$$

these are two-particle strange correlators in particle-hole and particle-particle channels, respectively, where  $S_{\mathbf{k}A}^{+} = \frac{1}{L} \sum_i e^{i\mathbf{k}\cdot\mathbf{R}_{i,A}} S_{i,A}^{+}$  and  $\Delta_{\mathbf{k}A}^{\dagger} = \frac{1}{L} \sum_i e^{i\mathbf{k}\cdot\mathbf{R}_{i,A}} \Delta_{i,A}^{\dagger}$ , with  $S_{i,A}^{+} = c_{i,A,\uparrow}^{\dagger} c_{i,A,\downarrow}$  flipping spin in sublattice  $A$  of unit cell  $i$ , and  $\Delta_{i,A}^{\dagger} = c_{i,A,\uparrow}^{\dagger} c_{i,A,\downarrow}^{\dagger}$  creating a Cooper pair of spin singlet in sublattice  $A$  of unit cell  $i$ .

Although the magnetic nature of the QSH to AFMI transition has been studied thoroughly<sup>35,40</sup>, here we find the topological nature of this transition is well captured by the strange correlators in single and two-particle sectors. As will be explained later, the QMC computation of strange correlator is more efficient and robust than the QMC simulations with either open boundary condition (OBC) to directly probe the edge modes<sup>33,34</sup>, or measurements of entanglement spectrum where one has to bifurcate the already small finite size system and analytical continue the imaginary time data<sup>22,23</sup>.

### III. NUMERICAL RESULTS AND DISCUSSIONS

#### A. Single-particle strange correlator

We first apply the single-particle strange correlator to detect the topological phase transition driven by  $t_d$  at noninteracting limit. In Fig. 3, we set  $U = 0$  but gradually increase  $t_d$  in  $|\Psi\rangle$ . One clearly sees that when  $t_d < 2t$ , the strange correlator  $|C_{\mathbf{k}AB}^{\uparrow}|$  is linearly divergent at one M point in the Brillouin zone, which is consistent with the prediction in Ref. 26. When  $t_d > 2t$ , both  $\langle \Omega | \Psi(t_d = 100t) \rangle$  and  $|\Psi(t_d > 2t)\rangle$  become topological trivial state ( $C_s = 0$ ), the divergence of  $|C_{\mathbf{k}AB}^{\uparrow}|$  is removed.  $1/|C_{\mathbf{k}AB}^{\uparrow}|$  shows a upturn behavior around  $\mathbf{k}_M$ .

Before we move on to strange correlator in the interacting case, we first look at the phase transition from QSH to AFMI from the magnetic perspective. Fig. 4 (a) shows the  $1/L$  extrapolation of antiferromagnetic structure factor

$$S_{AF}^{xy} = \frac{1}{4L^2} \sum_{\langle i,j \rangle} \sum_{\alpha=A,B} \langle S_{i,\alpha}^{+} S_{j,\alpha}^{-} + S_{i,\alpha}^{-} S_{j,\alpha}^{+} \rangle \quad (6)$$

for various values of  $U/t$ .  $\langle \dots \rangle$  means QMC average with  $|\Psi\rangle$  on both sides of the observable, hence,  $S_{AF}^{xy}$  is not measured as strange correlator but as regular QMC correlator. From the extrapolated values of  $L \rightarrow \infty$ , one can see the  $xy$  antiferromagnetic order sets in around  $U_c \approx 5.7t$  which is consistent with previous QMC results<sup>36,42</sup>. The corresponding magnetic moment is obtained as  $m_{xy} = \sqrt{S_{AF}^{xy}/L^2}$ , and its value is plotted as a

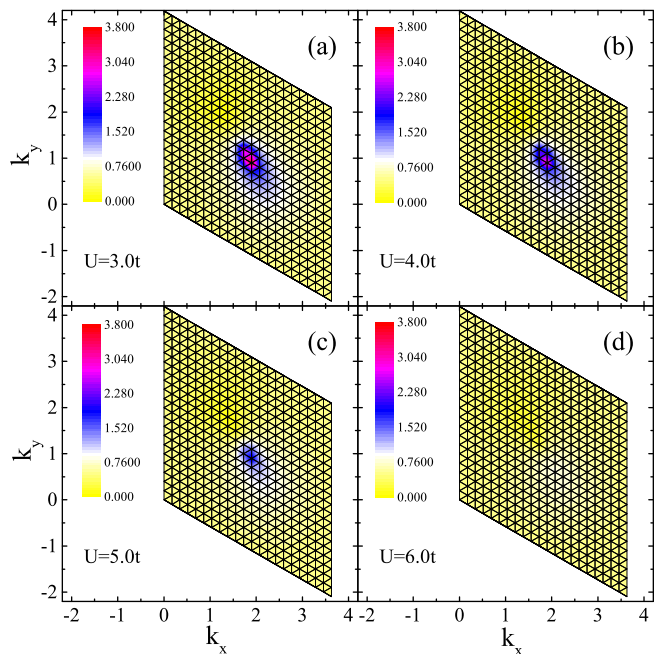


FIG. 5. (color online) The contour plot of single-particle strange correlator  $|C_{\mathbf{k}AB}^{\uparrow}|$  with increasing Hubbard interaction  $U/t$ . The finite system size used here is  $L = 21$ . The  $\mathbf{k}$ -space area in the four panels is the same as the dashed region in the inset of Fig. 2, which is the whole BZ.

function of  $U/t$  in Fig. 4 (b). The appearance of magnetic long-range order breaks the time-reversal symmetry and destroy the bulk topological state. Previous theoretical and numerical studies show that the counter propagating edge modes in the QSH phase are expected to become gapped exactly at the point where long-range magnetic order in the bulk breaks time-reversal symmetry<sup>44</sup>.

After determining the critical  $U_c$  from magnetic perspective, we monitor the single-particle strange correlator  $|C_{\mathbf{k}AB}^{\uparrow}|$  as a function of  $U/t$  in the whole Brillouin zone. For a global view, Fig. 5 shows the contour plot of strange correlator  $|C_{\mathbf{k}AB}^{\uparrow}|$  with increasing  $U/t$  for a fixed system size  $L = 21$ . When  $U$  is small, there is a clear singularity at one and only one of the time-reversal-symmetric M point. In the thermodynamic limit, the single-particle strange correlator is still divergent at one M point in Fig. 5 (a-c). When  $U > U_c$ , see Fig. 5 (d), there will be no divergence in the single-particle strange correlator.

A careful analysis of  $1/|C_{\mathbf{k}AB}^{\uparrow}|$  along the high-symmetry path  $\text{K} \rightarrow \text{M} \rightarrow \text{G}$  is shown in Fig. 6. In Fig. 6 (a-d), the single-particle strange correlator still shows divergent tendency at M point with the finite system size up to  $L = 27$ . When  $U > U_c$ , see Fig. 6 (e) and (f), where the detected target state  $|\Psi\rangle$  becomes topologically trivial, we clearly see the upturn behavior around M point in  $1/|C_{\mathbf{k}AB}^{\uparrow}|$ .

To give a better understanding of the results in Fig. 6, we turn to the helical Luttinger liquid theory. Based on the space-time rotation interpretation of the strange

correlator, we can analyze the single-particle strange correlator using the helical Luttinger liquid theory at the (1+1)D boundary<sup>45–48</sup>, according to which, the real-space strange correlator in the single-particle sector scales as

$$C_{\mathbf{r}AB}^\sigma \sim \mathbf{r}^{-g/2-1/2g}, \quad (7)$$

where  $g$  is the Luttinger parameter related to  $U/t$ ,  $g \in [0, 1]$ . After Fourier transform to the momentum space, it becomes

$$C_{\mathbf{k}AB}^\sigma \sim \tilde{\mathbf{k}}^{g/2+1/2g-2}, \quad (8)$$

where  $\tilde{\mathbf{k}} = |\mathbf{k} - \mathbf{k}_M|$ . Unlike the noninteracting case, the single-particle strange correlator in the momentum space may actually stop diverging before the QSH to AFMI transition point. To see this point more clearly, the critical  $g_c$  can be solved from the equation  $g/2+1/2g-2=0$ ,

which gives  $g_c = 2 - \sqrt{3} \approx 0.268$ . If  $g < g_c$ , there would be no divergent behavior around the M point in the momentum space of single-particle strange correlator, although the real space strange correlator still obeys a power-law decay. For  $g > g_c$ , the power-law divergent behavior of the single-particle strange correlator around the M point clearly signifies that the interacting QSH phase and the trivial band insulator belongs to distinct SPT phases, and the two states must be separated by gapless fermion edge modes when they are adjacent in the space. From the data in Fig. 6, the divergent behavior persists up to  $U = 5.5t$ , which is very close to the quantum critical point extracted from previous QMC simulations. From Fig. 6 here and Fig. 8 in Sec. III B, we can see that the divergent exponent of single-particle strange correlator is reduced by the interaction which cannot be captured by noninteracting topological phase transition in Fig. 3 and clearly beyond the mean-field level.

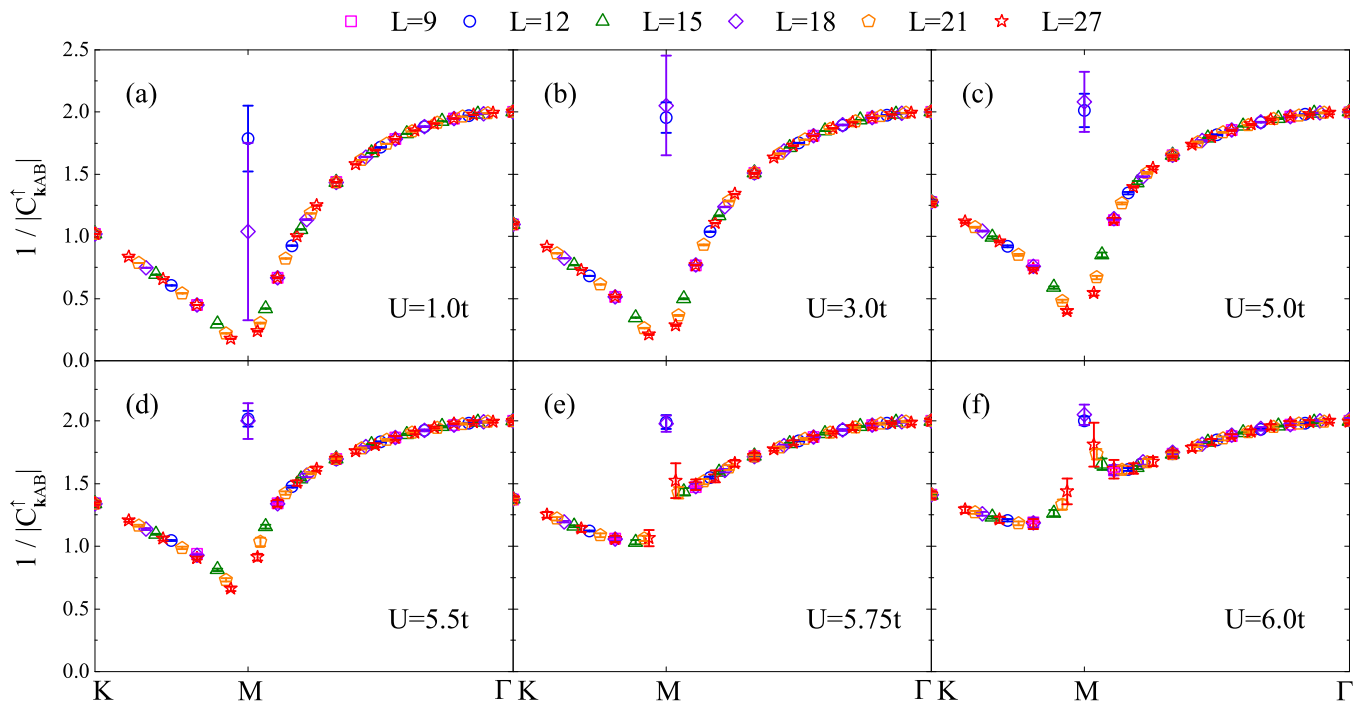


FIG. 6. (color online) The inverse amplitude of single-particle strange correlator  $1/|C_{\mathbf{k}AB}^\dagger|$  along high-symmetry path for various  $U/t$  and system sizes. When the interaction  $U/t \leq 5.5t$ , see (a-d), there is a divergent tendency in  $|C_{\mathbf{k}AB}^\dagger|$  around M point. However, the divergent exponent is reduced due to the correlation effects according to the helical Luttinger liquid theory (see the main text). In the AFMI regime (e-f),  $1/|C_{\mathbf{k}AB}^\dagger|$  shows upturn behavior around M point. there is no divergence at all.

We notice that the data points exactly at  $\mathbf{k} = \mathbf{k}_M$  in Fig. 6 (a-d) suddenly jump up and have larger errorbars. This is unphysical, and we will discuss the behavior of  $C_{\mathbf{k}AB}^\dagger$  in the presence of small AF order  $\Delta_{\text{SDW}}$  around the M point in a mean-field context in Appendix A, where this unphysical singularity at  $\mathbf{k} = \mathbf{k}_M$  will be understood.

We want to stress that based on the Luttinger liquid theory the single-particle strange correlator, and equivalently the single particle Green's function at the physical

edge of the system always follow a power-law decay, before the system develops a true long range order in the bulk. This is mainly because that when the bulk is fully gapped, all the low energy physics occur at the boundary of the system. Then based on the Mermin-Wagner theorem<sup>49</sup>, continuous symmetries cannot be spontaneously broken in a (1 + 1)D system, and without a true long range correlation of magnetic or superconductor order parameter, the fermions at the boundary should remain

gapless (though still strongly interacting).

The technical advantage of strange correlator in QMC over other numerical diagnoses of interacting TIs is manifestly presented, i.e., we have performed simulations on finite size system with periodic boundary condition (PBC), yet, still are able to extract information of the edge modes which, in the past, could only be obtained with systems with OBC<sup>33,34</sup>. It is well known that QMC simulations with OBC suffer from greater finite size effect, apparently, strange correlator avoids this difficulty. Moreover, direct probe of edge modes with OBC requires analytical continuation of imaginary time Green's function, i.e., from  $G(\mathbf{k}, \tau)$  to  $A(\mathbf{k}, \omega)$ , and that usually renders ambiguity in the real-frequency data. However, with strange correlator, we only need to measure static (equal

time) single-particle Green's function in PBC system, which is the easiest and most reliable observables in the QMC simulations. Thirdly, as mentioned in the Introduction, in comparison with measurements of entanglement spectrum to detect the interaction-driven topological transition<sup>21-23</sup>, strange correlator is also physically more transparent and technically more robust, as in the entanglement spectrum measurements one has to bifurcate the already small finite size system and analytically continue the imaginary time data, whereas in the strange correlator both problems are avoided. Hence, at the technical level, to the best of our knowledge, strange correlator is indeed the easiest diagnosis of the topological states and the topological quantum phase transition in interacting systems.

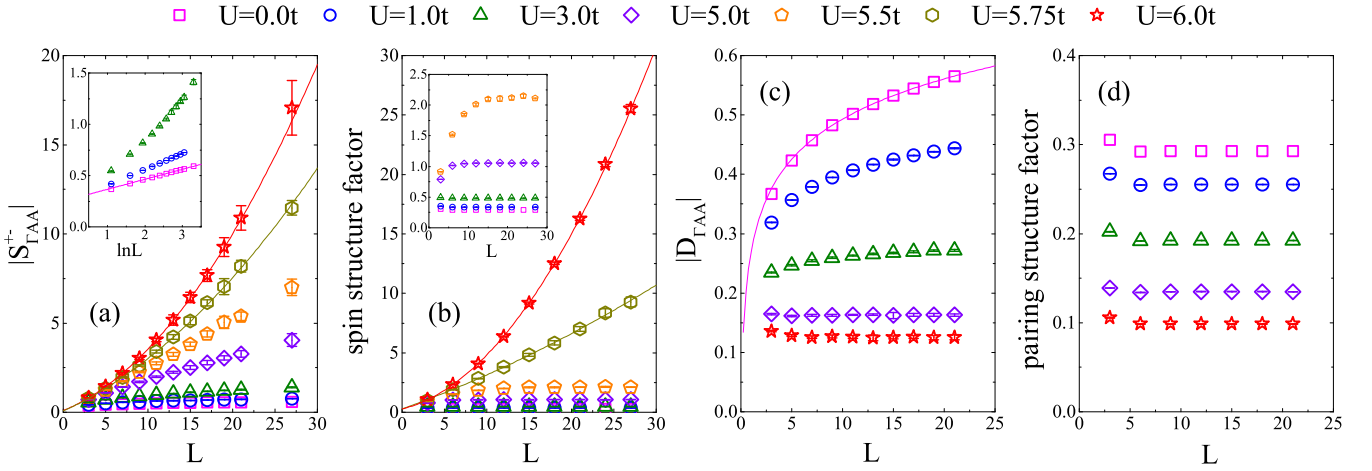


FIG. 7. (color online) (a), (c) spin and pairing strange correlators  $|S_{\Gamma AA}^{\pm}|$  and  $|D_{\Gamma AA}|$  as a function of system size  $L$  for various  $U/t$ . The inset of (a) is a zoomin at small  $U/t$ , with a logarithmic fit (magenta solid line) of the data at  $U = 0$  according to Eq. 13. The apple green and red solid lines in the main panel of (a) are power-law fits according to Eq. 15 at  $U = 5.75t (\sim U_c)$  and  $U = 6t$ . The logarithmic fit (magenta solid line) in (c) also follows Eq. 14 at  $U = 0$ . (b), (d) spin and pairing regular correlation functions  $\langle \Psi | S_k^+ S_k^- | \Psi \rangle$  and  $\langle \Psi | \Delta_k^+ \Delta_k | \Psi \rangle$  as a function of  $L$  for various  $U/t$ . The apple green and red solid lines in (b) are power-law fits according to Eq. 15 at  $U = 5.75t (\sim U_c)$  and  $U = 6t$ . The inset of (b) is a zoomin of the regular spin structure factor at small  $U/t$ , showing that they are independent of  $L$  when  $U < U_c$ .

## B. Two-particle strange correlators

In this section, we discuss the QMC results on strange correlators in two-particle sector, i.e., the spin and pairing strange correlators in the presence of interaction.

Again, based on the space-time rotation interpretation of the strange correlator, we can likewise analyze the spin and pairing strange correlators using the helical Luttinger liquid theory at the (1+1)D boundary<sup>45-48</sup>. According to the theory, the real-space strange correlator in the spin and pairing sectors scale as

$$S_{\mathbf{r}AA}^{\pm} \sim \mathbf{r}^{-2g}, \quad (9)$$

$$D_{\mathbf{r}AA} \sim \mathbf{r}^{-2/g}, \quad (10)$$

where  $g$  is the Luttinger parameter. After Fourier trans-

form to the momentum space, they become

$$S_{\mathbf{k}AA}^{\pm} \sim \tilde{\mathbf{k}}^{2g-2}, \quad (\sim L^{2-2g} \text{ at } \mathbf{k} = \Gamma), \quad (11)$$

$$D_{\mathbf{k}AA} \sim \tilde{\mathbf{k}}^{2/g-2}, \quad (\sim L^{2-2/g} \text{ at } \mathbf{k} = \Gamma). \quad (12)$$

where  $\tilde{\mathbf{k}} = |\mathbf{k} - \mathbf{k}_{\Gamma}|$ . In the non-interacting limit ( $U=0$ )  $g = 1$ , and as we increase  $U/t$  towards  $U_c$ ,  $g$  will become smaller and smaller, eventually vanish at the transition point.

To better understand the behavior in each limit, let us start with  $g = 1$  ( $U = 0$ ), and we have

$$S_{\mathbf{k}AA}^{\pm} \sim \tilde{\mathbf{k}}^0 \sim \ln(\mathbf{k}), \quad (\sim \ln(L) \text{ at } \mathbf{k} = \Gamma), \quad (13)$$

$$D_{\mathbf{k}AA} \sim \tilde{\mathbf{k}}^0 \sim \ln(\mathbf{k}), \quad (\sim \ln(L) \text{ at } \mathbf{k} = \Gamma). \quad (14)$$

Such a logarithmic growth in  $L$  fits our calculated data in Fig. 7 (a) and (c) for the  $U = 0$  cases very well. The logarithmic growth is in strong contrast to the regular

spin and pairing correlators, as shown in Fig. 7 (b) and (d), which, at  $U = 0$ , are independent of system size  $L$ , meaning both spin and pairing correlations are exponentially short-ranged in real space, corresponding to the QSH insulator with a bulk gap.

On the other hand, near the QSH to AFMI transition point,  $g = 0$  ( $U \sim U_c$ ), we have

$$S_{\mathbf{k}AA}^{\pm} \sim \tilde{\mathbf{k}}^{-2}, \quad (\sim L^2 \text{ at } \mathbf{k} = \Gamma), \quad (15)$$

$$D_{\mathbf{k}AA} \sim \tilde{\mathbf{k}}^{\infty}, \quad (\sim L^{-\infty} \sim e^{-L} \text{ at } \mathbf{k} = \Gamma). \quad (16)$$

As we can see, the calculated data in Fig. 7 (a) at  $U = 6t$  indeed diverge as  $L^2$  in the thermodynamic limit. More interestingly, such a divergence is the same as the one shown by the regular spin correlator inside the AFMI phase, as shown in Fig. 7 (b) at  $U = 6t$ . This is because when  $U = 6t$ , the ground state wavefunction  $|\Psi\rangle$  in Eq. 4 is already in the AFMI phase, the spin strange correlator is then equal to the spin regular correlator in the sense that it picks up the long-range spin correlation. In Fig. 7 (c) at  $U = 6t$ , the pairing strange correlator decays exponentially to a constant, also consistent with the prediction in Eq. 16.

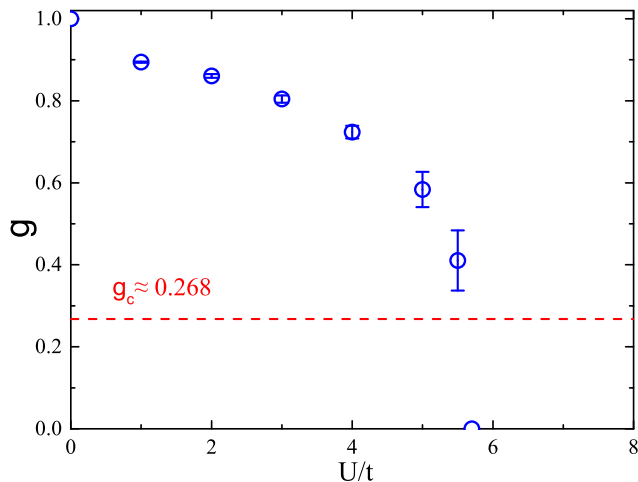


FIG. 8. (color online) The Luttinger parameter  $g$  extracted from the spin strange correlator in Fig. 7 (a) following Eq. 11. Below the critical value  $g_c$ , the single-particle strange correlator in the momentum space is no longer divergent at M point.

Between the limits of  $g = 1$  ( $U = 0$ ) and  $g = 0$  ( $U = U_c$ ), we can fit spin and pairing strange correlator data in Fig. 7 (a) and (c), with the Luttinger liquid theory prediction in Eq. 11 and 12, to extract the Luttinger parameter  $g$ . The extracted  $g$  values as a function of  $U/t$  are shown in Fig. 8, one can see that  $g$  continuously decreases from 1 to 0, which accounts for the increasing electron-electron correlation. The dashed line in Fig. 8 highlights the  $g_c$  smaller than which the single-particle strange correlator stop diverging, as discussed in Sec. III A.

## IV. SUMMARY AND OUTLOOK

In summary, we have employed large-scale QMC simulations to study the single- and two-particle strange correlators in a realistic model for interacting topological insulators. We demonstrate that the interaction driven topological-trivial insulator quantum phase transition can be well captured by the strange correlators. Although larger system sizes might be needed for detailed information very close to the critical point, our results show that the strange correlator is a powerful and promising tool to diagnose topological insulator with interaction.

The technical advantage of strange correlator in numerical studies (especially QMC simulations) on interacting fermionic and bosonic SPT states are obvious. As one only needs to measure static correlations in the bulk system, there is no need to apply OBC to actually probe the spatial edges, no need to apply analytical continuation to access real frequency data, and no need to bifurcate the already small finite size systems for entanglement measurements. In short, the strange correlator is much easier to implement and robust in practical numerical performance.

As for future applications, the QSH insulator discussed in our work has a full spin  $S^z$  conservation, which has a  $\mathbb{Z}$  classification instead of a  $\mathbb{Z}_2$  classification for the cases with time-reversal symmetry but no  $S^z$  conservation. In Ref. 26 the strange correlator was tested for a noninteracting QSH insulator with a sizable Rashba spin-orbit coupling, which does have a  $\mathbb{Z}_2$  classification. We expect the same strange correlator is still applicable to the interacting QSH insulator with Rashba spin-orbit coupling as well, except now that the two electron operators in the strange correlator Eq. 3 do not have to have the same spin, since the spin conservation is broken by the Rashba term.

As we mentioned in the introduction, in all dimensions interaction can change or reduce the classification of some topological insulators, for example, interaction may trivialize some topological insulators that are nontrivial in the noninteracting limit. This means that in this case the strange correlator should be power-law or long range correlated without interaction, but becomes short-ranged due to interaction, possibly even *without* going through any bulk phase transition. We will leave this to future study.

## ACKNOWLEDGMENTS

The numerical calculations were carried out at the Physical Laboratory of High Performance Computing in RUC as well as the National Supercomputer Center in Guangzhou on the platform Tianhe-2. HQW, YYH and ZYL acknowledge support from National Natural Science Foundation of China (Grant Nos. 11474356 and 91421304) and National Program for Basic Research of

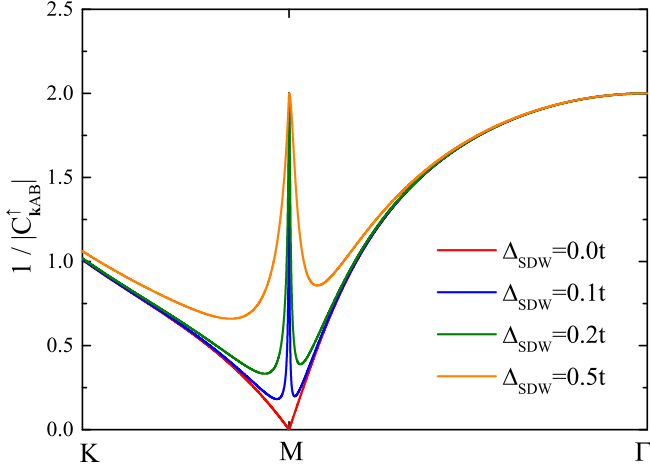


FIG. 9. The inverse strange correlator  $1/|C_{\mathbf{k}AB}^\dagger|$  along the high-symmetry path in the mean field theory. The state  $|\Psi\rangle$  is replaced by an SDW insulator controlled by  $\Delta_{\text{SDW}}$ .

MOST of China (Grant No. 2011CBA00112). CX and ZY are supported by the David and Lucile Packard Foundation and NSF Grant No. DMR-1151208. ZYM is supported by the National Thousand-Young-Talents Program of China.

### Appendix A: A Mean-Field Calculation of the Strange Correlator

To facilitate the understanding of the behavior of single-particle strange correlator in the QSH insulator to  $xy$  AFMI transition in the KMH model, below, we also provide a mean field level calculation of  $1/|C_{\mathbf{k}AB}^\dagger|$  by introducing the spin density wave (SDW) order parameter,  $\Delta_{\text{SDW}}$ . The mean field Hamiltonian can be written as

$$H_{\text{MF}} = - \sum_{\langle ij \rangle, \sigma} t_{ij} c_{i\sigma}^\dagger c_{j\sigma} + i\lambda \sum_{\langle\langle ij \rangle\rangle, \alpha, \beta} v_{ij} c_{i\alpha}^\dagger \sigma_{\alpha\beta}^z c_{j\beta} - \Delta_{\text{SDW}} \sum_{i, \alpha, \beta} (-)^i c_{i\alpha}^\dagger \sigma_{\alpha\beta}^x c_{i\beta}, \quad (\text{A1})$$

where  $\Delta_{\text{SDW}}$  is the SDW gap. Here we set  $\lambda = 0.2t$ . If  $t_d = t$  and  $\Delta_{\text{SDW}} = 0$ ,  $H_{\text{MF}}$  describes the QSH insulator. The trivial band insulator can be obtained by tuning  $t_d > 2t$ . The strong interacting AFMI can be phenomenologically modeled by a finite  $\Delta_{\text{SDW}}$  term in the mean-field theory, which breaks the spin  $U(1)$  symmetry and describes the spin ordered antiferromagnetic

state. Here we assume the  $xy$  spin order lies in the spin- $x$  direction.

We calculated the inverse strange correlator  $1/|C_{\mathbf{k}AB}^\dagger|$  with the state  $|\Psi\rangle$  tuned by the mean-field parameter  $\Delta_{\text{SDW}}$ . The result is shown in Fig. 9. When  $\Delta_{\text{SDW}} = 0$ ,  $|\Psi\rangle$  is the QSH state, the inverse strange correlator  $1/|C_{\mathbf{k}AB}^\dagger| \sim |\mathbf{k} - \mathbf{k}_M|$  follows the linear behavior around the M point, which implies the power law behavior of the strange correlator  $|C_{\mathbf{k}AB}^\dagger| \sim |\mathbf{k} - \mathbf{k}_M|^{-\alpha}$  with  $\alpha = 1$ . However, beyond the mean field theory, the interaction can modify this power  $\alpha$ , so the strange correlator can deviate from the  $\alpha = 1$  behavior in the momentum space, as shown in Eq. 8 and Fig. 8 in the main text. But the power law behavior of the strange correlator in the real space is still expected to survive in the whole QSH phase.

As  $\Delta_{\text{SDW}}$  is turned on,  $1/|C_{\mathbf{k}AB}^\dagger|$  will be lifted from zero at the M point and replaced by a small peak. The stronger SDW order will lead to the earlier upturn of the curve as approaching to the M point. The upturn behavior around the M point can be described by

$$C_{\mathbf{k}AB}^\dagger = \frac{(k + im_\Omega)(\Delta_{\text{SDW}}^2 m_\Omega + k(k - im_\Psi)(m_\Omega + m_\Psi))}{2(\Delta_{\text{SDW}}^2 m_\Omega^2 + k^2(m_\Omega + m_\Psi)^2)}, \quad (\text{A2})$$

where  $k = v_F|\mathbf{k} - \mathbf{k}_M|$  is the small momentum deviation from the M point,  $m_\Omega$  and  $m_\Psi$  are respectively the single-particle mass gaps in the trivial state  $|\Omega\rangle$  and the QSH state  $|\Psi\rangle$ . Eq. A2 is derived by small momentum expansion around the M point. As can be seen from the denominator, the power law divergence of the strange correlator  $|C_{\mathbf{k}AB}^\dagger|$  (as  $k \rightarrow 0$ ) will be removed once the SDW order  $\Delta_{\text{SDW}}$  sets in at the topological transition to the AFMI phase. What's more, according to Eq. A2, the limit of  $\Delta_{\text{SDW}} \rightarrow 0$  and the limit of  $\mathbf{k} \rightarrow \mathbf{k}_M$  do not commute:

$$\lim_{k \rightarrow 0} C_{\mathbf{k}AB}^\dagger = \frac{i}{2}, \quad \lim_{\Delta_{\text{SDW}} \rightarrow 0} C_{\mathbf{k}AB}^\dagger = \frac{(k + im_\Omega)(k - im_\Omega)}{k(m_\Omega + m_\Psi)} \sim \frac{1}{k}, \quad (\text{A3})$$

If one takes  $\Delta_{\text{SDW}} \rightarrow 0$  first, then the strange correlator  $C_{\mathbf{k}AB}^\dagger$  indeed follows the  $1/k$  power-law behavior as expected on the mean-field level. However, in our QMC simulation, we take  $k \rightarrow 0$  first due to the presence of the AF fluctuations as a result of the finite-size effect, so the strange correlator  $C_{\mathbf{k}AB}^\dagger$  approaches to another limit  $i/2$ , which is not divergent. It is this non-commutative limit that makes  $|C_{\mathbf{k}AB}^\dagger|$  ill-defined at the M point and the data right at the M point meaningless in Fig. 3 (a-d). Only when the interaction becomes sufficiently strong (the Luttinger parameter  $g < g_c$ ), so that the divergence at  $\mathbf{k}_M$  is removed, and the data of  $1/|C_{\mathbf{k}AB}^\dagger|$  at  $\mathbf{k} = M$  becomes meaningful.

\* zymeng@iphy.ac.cn

<sup>1</sup> X. Chen, Z.-C. Gu, Z.-X. Liu, and X.-G. Wen,

- Phys. Rev. B* **87**, 155114 (2013).
- <sup>2</sup> X. Chen, Z.-C. Gu, Z.-X. Liu, and X.-G. Wen, *Science* **338**, 1604 (2012).
  - <sup>3</sup> A. P. Schnyder, S. Ryu, A. Furusaki, and A. W. W. Ludwig, *AIP Conference Proceedings* **1134**, 10 (2009).
  - <sup>4</sup> S. Ryu, A. P. Schnyder, A. Furusaki, and A. W. W. Ludwig, *New Journal of Physics* **12**, 065010 (2010).
  - <sup>5</sup> A. Kitaev, *AIP Conference Proceedings* **1134**, 22 (2009).
  - <sup>6</sup> D. J. Thouless, M. Kohmoto, M. P. Nightingale, and M. den Nijs, *Phys. Rev. Lett.* **49**, 405 (1982).
  - <sup>7</sup> C. L. Kane and E. J. Mele, *Phys. Rev. Lett.* **95**, 146802 (2005).
  - <sup>8</sup> C. L. Kane and E. J. Mele, *Phys. Rev. Lett.* **95**, 226801 (2005).
  - <sup>9</sup> L. Fidkowski and A. Kitaev, *Phys. Rev. B* **81**, 134509 (2010).
  - <sup>10</sup> L. Fidkowski and A. Kitaev, *Phys. Rev. B* **83**, 075103 (2011).
  - <sup>11</sup> X.-L. Qi, *New Journal of Physics* **15**, 065002 (2013).
  - <sup>12</sup> H. Yao and S. Ryu, *Phys. Rev. B* **88**, 064507 (2013).
  - <sup>13</sup> S. Ryu and S.-C. Zhang, *Phys. Rev. B* **85**, 245132 (2012).
  - <sup>14</sup> Z.-C. Gu and M. Levin, *Phys. Rev. B* **89**, 201113 (2014).
  - <sup>15</sup> L. Fidkowski, X. Chen, and A. Vishwanath, *Phys. Rev. X* **3**, 041016 (2013).
  - <sup>16</sup> C. Wang and T. Senthil, *Phys. Rev. B* **89**, 195124 (2014).
  - <sup>17</sup> Y.-Z. You, Y. BenTov, and C. Xu, *arXiv* **1402**, 4151 (2014).
  - <sup>18</sup> Y.-Z. You and C. Xu, *Phys. Rev. B* **90**, 245120 (2014).
  - <sup>19</sup> Y.-Z. You and C. Xu, *Phys. Rev. B* **91**, 125147 (2015).
  - <sup>20</sup> H. Li and F. D. M. Haldane, *Phys. Rev. Lett.* **101**, 010504 (2008).
  - <sup>21</sup> T. Grover, *Phys. Rev. Lett.* **111**, 130402 (2013).
  - <sup>22</sup> F. F. Assaad, T. C. Lang, and F. Parisen Toldin, *Phys. Rev. B* **89**, 125121 (2014).
  - <sup>23</sup> F. F. Assaad, *Phys. Rev. B* **91**, 125146 (2015).
  - <sup>24</sup> M. Jarrell and J. Gubernatis, *Physics Reports* **269**, 133 (1996).
  - <sup>25</sup> K. Beach, *arXiv:cond-mat* **0403055** (2004).
  - <sup>26</sup> Y.-Z. You, Z. Bi, A. Rasmussen, K. Slagle, and C. Xu, *Phys. Rev. Lett.* **112**, 247202 (2014).
  - <sup>27</sup> L. Fu, *Phys. Rev. Lett.* **106**, 106802 (2011).
  - <sup>28</sup> K. Wierschem and P. Sengupta, *Phys. Rev. Lett.* **112**, 247203 (2014).
  - <sup>29</sup> K. Wierschem and P. Sengupta, *Phys. Rev. B* **90**, 115157 (2014).
  - <sup>30</sup> T. Scaffidi and Z. Ringel, *arXiv* **1505**, 02775 (2015).
  - <sup>31</sup> F. Assaad and H. Evertz, in *Computational Many-Particle Physics*, Lecture Notes in Physics, Vol. 739, edited by H. Fehske, R. Schneider, and A. Weiße (Springer Berlin Heidelberg, 2008) pp. 277–356.
  - <sup>32</sup> F. D. M. Haldane, *Phys. Rev. Lett.* **61**, 2015 (1988).
  - <sup>33</sup> M. Hohenadler, T. C. Lang, and F. F. Assaad, *Phys. Rev. Lett.* **106**, 100403 (2011).
  - <sup>34</sup> D. Zheng, G.-M. Zhang, and C. Wu, *Phys. Rev. B* **84**, 205121 (2011).
  - <sup>35</sup> M. Hohenadler, Z. Y. Meng, T. C. Lang, S. Wessel, A. Muramatsu, and F. F. Assaad, *Phys. Rev. B* **85**, 115132 (2012).
  - <sup>36</sup> F. F. Assaad, M. Bercx, and M. Hohenadler, *Phys. Rev. X* **3**, 011015 (2013).
  - <sup>37</sup> T. C. Lang, A. M. Essin, V. Gurarie, and S. Wessel, *Phys. Rev. B* **87**, 205101 (2013).
  - <sup>38</sup> H.-H. Hung, L. Wang, Z.-C. Gu, and G. A. Fiete, *Phys. Rev. B* **87**, 121113 (2013).
  - <sup>39</sup> H.-H. Hung, V. Chua, L. Wang, and G. A. Fiete, *Phys. Rev. B* **89**, 235104 (2014).
  - <sup>40</sup> Z. Y. Meng, H.-H. Hung, and T. C. Lang, *Modern Physics Letters B* **28**, 1430001 (2014).
  - <sup>41</sup> S. Rachel and K. Le Hur, *Phys. Rev. B* **82**, 075106 (2010).
  - <sup>42</sup> F. Parisen Toldin, M. Hohenadler, F. F. Assaad, and I. F. Herbut, *Phys. Rev. B* **91**, 165108 (2015).
  - <sup>43</sup> It is well-known that most topological insulators can be described by Dirac fermions at low energy, and the bosonic SPT states can be described by either a nonlinear sigma model field theory<sup>50</sup>, or a Chern-Simons field theory<sup>51</sup>, both of which have an effective Lorentz invariance.
  - <sup>44</sup> M. Hohenadler and F. F. Assaad, *Journal of Physics: Condensed Matter* **25**, 143201 (2013).
  - <sup>45</sup> C. Xu and J. E. Moore, *Phys. Rev. B* **73**, 045322 (2006).
  - <sup>46</sup> C. Wu, B. A. Bernevig, and S.-C. Zhang, *Phys. Rev. Lett.* **96**, 106401 (2006).
  - <sup>47</sup> C.-H. Chung, D.-H. Lee, and S.-P. Chao, *Phys. Rev. B* **90**, 035116 (2014).
  - <sup>48</sup> M. Hohenadler and F. F. Assaad, *Journal of Physics: Condensed Matter* **25**, 143201 (2013).
  - <sup>49</sup> N. D. Mermin and H. Wagner, *Phys. Rev. Lett.* **17**, 1133 (1966).
  - <sup>50</sup> Z. Bi, A. Rasmussen, K. Slagle, and C. Xu, *Phys. Rev. B* **91**, 134404 (2015).
  - <sup>51</sup> Y.-M. Lu and A. Vishwanath, *Phys. Rev. B* **86**, 125119 (2012).